Title

NUCLEON AND NUCLEAR CROSS SECTIONS FOR POSITIVE PIONS AMD PROTONS ABOVE 1.4 Bev/c

Authors

Longo, Michael J.
Moyer, Burton J.

Publication Date

1961-08-01

UCRL -9497 Rev.

UNIVERSITY OF CALIFORNIA

Ernest O. Lawrence Radiation Laboratory

BERKELEY, CALIFORNIA

DISCLAIMER

UCRL-9497 Rev.
Limited distribution

UNIVERSITY OF CALIFORNIA
Lawrence Radiation Laboratory
Berkeley, California

Contract No. W-7405-eng-48

NUCLEON AND NUCLEAR CROSS SECTIONS FOR POSITIVE PIONS AND PROTONS ABOVE 1.4 Bev/c

Michael J. Longo and Burton J. Moyer

August 1, 1961

NUCLEON AND NUCLEAR CROSS SECTIONS FOR POSITIVE PIONS AND PROTONS ABOVE 1.4 Bev/c */

Michael J. Longo and Burton J. Moyer

Lawrence Radiation Laboratory

University of California

Berkeley, California

August 1, 1961

ABSTRACT

1. Total (π^+,p) and (p,p) cross sections in the momentum range 1.4 to 4.0 Bev/c are presented. These measurements, with an accuracy of approximately 2%, were made at the Berkeley Bevatron by using counter techniques. Pions were distinguished from protons by means of a gas-filled Cerenkov counter. The (π^+,p) total cross section was found to be almost constant above 2.0 Bev/c at a value near 29 mb. The (p,p) cross section decreases gradually from 47.5 mb to 41.7 mb over the momentum range covered.

2. Transmission measurements of π^+-nucleus and p-nucleus cross sections in both good and poor geometry were made at 3.0 Bev/c. The results are compared with the predictions of the optical model. In contrast to most previous work at high energies, an essentially exact solution of the wave equation for a potential well with a diffuse edge was used. The values of the imaginary part of the optical potential that best fit the experimental data are in good agreement with the predicted values. No strong conclusion regarding the real part of the potential was possible. Absorption and total elastic cross sections for Be, C, Al, and Cu are presented. The total elastic cross sections from this experiment disagree with Wikner's for π^--nucleus scattering.

I. INTRODUCTION

The pion-nucleon total cross section is well known for pion momenta below approximately 2.0 Bev/c, but little accurate data are available at higher momenta, especially for π^+-p scattering. We present here the results of a measurement of the total π^+-p cross section in the momentum range 1.4 to 4.0 Bev/c.[1] Total p-p cross sections were measured simultaneously in the same momentum range. These measurements, with accuracy of approximately 2%, were made at the Berkeley Bevatron, by using counter techniques, and are part of an experimental program whose objective is a detailed knowledge of the pion-nucleon interaction above 500 Mev.

It was also possible in this experiment to measure cross sections for several heavy nuclei with the same equipment used to measure the total π^+-p and p-p cross sections. This was done at 3.0 Bev/c for Be, C, Al, and Cu with various geometries. The results are used to determine best-fit values of the imaginary part of the nuclear potential, which are then compared with the predictions of the optical model.

In contrast to most previous attempts to make fits of this type to high-energy scattering data, those presented here were made by using an essentially exact solution of the wave equation for a complex potential well with a diffuse edge. This was possible through the use of a high-speed electronic computer (the IBM 704).

II. EXPERIMENTAL METHOD AND EQUIPMENT

A. General Description of Method

In these measurements, a beam consisting primarily of a mixture of positive pions and protons of well-defined momentum was collimated by means of a counter telescope. Pions were separated from protons electronically by use of a gas-filled Cerenkov counter. This allowed simultaneous

measurements of pion and proton cross sections. After passing through the monitor telescope, the beam was allowed to strike an absorber. The fraction of beam transmitted was determined by means of a counter placed after the absorber. The apparent cross section is a function of θ, the half-angle subtended by the edge of this transmission counter. In the idealized experiment we are discussing, the apparent cross section $\sigma(\theta)$ is given by

$$\sigma(\theta) = - \frac{1}{nx} \log N/N_0, \qquad (1)$$

where N/N_0 is the fraction of beam transmitted for a particular value of θ, and nx is the number of nuclei per cm^2 as seen by the incoming beam. The expected variation of $\sigma(\theta)$ with the solid angle subtended by the transmission counter is depicted in Fig. 1. At very small angles the curve rises sharply because of Coulomb scattering (portion AB of the curve). As θ is increased, a point is reached where most of the Coulomb scattering is contained, but the majority of particles undergoing nuclear interactions are scattered out of the cone subtended by the detector (Point B). It is instructive to note here that the slope of such a plot of $\sigma(\theta)$ vs solid angle in the region BCD is $(d\sigma/d\Omega)_{el}$, the differential elastic cross section.[2] At high energies the elastic scattering is strongly peaked forward, with an angular distribution characteristic of diffraction scattering. Most of the elastic scattering is therefore confined to angles $\lesssim (kR)^{-1}$, where k is the wave number of the incident particle, and R is the radius of the nucleus. Thus, for $\theta \gg (kR)^{-1}$, the curve for $\sigma(\theta)$ is almost flat and approximately equal to the inelastic cross section (region DE in Fig. 1).

Measurements of $\sigma(\theta)$ in this experiment were made over this entire range of angles for beryllium, carbon, aluminum, and copper absorbers, with

3.0-Bev/c pions and protons. For hydrogen, measurements were made only in the region BC in Fig. 1 because of the large angles involved. This part of the curve can be extrapolated to $\theta = 0$ to give the total nuclear cross section.

The technique used for the hydrogen and heavy-nuclei measurements were basically the same. Each measurement consisted of a cycle of runs with target full (or target in), preceded and followed by target-empty runs. A complete cycle generally lasted about 4 hours. Successive runs were compared for reproducibility to check equipment operation. Frequent checks were also made with a test pulser.

B. Beam Geometry

The over-all experimental arrangement is shown in Fig. 2. It is unusual in that the apparatus was set up on the inside of the Bevatron ring in order to obtain a positive pion beam of as high-momentum as possible. The production of high-energy particles at the Bevatron target is strongly peaked forward so that it is necessary to take off a high-energy beam at a small angle from the circulating proton beam. The positive secondary particles are then bent inward toward the center of the Bevatron by the magnetic field. In this experiment, the take-off angles ranged from about +10 deg at 1.4 Bev/c to -15 deg at 4.0 Bev/c (positive angles measured outward away from the center of the Bevatron).

The orbits of the particles in the Bevatron were determined through an IBM-650 computer program, together with measured magnetic field profiles. At each momentum, rays that connect the target and point P in Fig. 2 were found, essentially by a process of trial and error. The currents required in the 12x60-in. bending magnet to deflect these "rays" through the proper angles were then determined by wire-orbit measurements.

Concrete shielding, only some of which is shown in Fig. 2, was used to minimize background in the counters. Where platform loading limitations prohibited the use of concrete shielding, paraffin blocks were used. Extensive magnetic shielding (not shown in Fig. 2) reduced the stray magnetic field along the beam line to a negligible value. This stray field without magnetic shielding varied from a few gauss to a few hundred gauss, depending on the proximity to the Bevatron magnet yoke.

Immediately following the 12x60-in. magnet was an 8-in.-bore doublet quadrupole whose main function was to increase the solid angle accepted by the counter telescope. Following the quadrupole was an 8-ft iron collimator with a 2-in. bore. This stopped most of the beam particles that missed the first monitor counter (M_1) and also provided magnetic shielding for that part of the beam line closest to the Bevatron magnet. A second bending magnet with an 18x36-in. pole tip was used to bend the beam away from the Bevatron structure. This considerably simplified the magnetic shielding problem along the latter part of the beam line.

The uncertainty in the beam momentum is estimated to be about $\pm 2\%$. The momentum spread in the beam was $\pm 2.5\%$ about the central momentum. Most of this spread resulted from the change in the Bevatron's magnetic field during the time the proton beam was spilled onto the target (150 msec).

C. The Counter System

The monitor telescope consisted of scintillation counters M_1, M_2, and M_3 and a gas Cerenkov counter C. All scintillators consisted of machined discs of polystyrene with 3% terphenyl. Counters M_1 and M_2 were each 1.5-in. in diameter; M_3 was 1-in. in diameter. The total length of the monitor telescope was 16-ft. Construction and operation of the gas Cerenkov counter have been described elsewhere.[3] In this experiment it was filled with sulfur hexafluoride to a pressure of 10 atm (absolute). This gave a

threshold velocity of 0.992 c and allowed a complete separation of pions and protons over the energy range of this experiment. A quadruple coincidence in M_1, M_2, C, and M_3 was required for a pion, and a triple coincidence between M_1, M_2, and M_3, with C in anticoincidence, was required for a proton count.

Absorbers were placed in the beam behind M_3. The fraction of the beam transmitted was measured at three solid angles simultaneously by scintillation counters S_1, S_2, and S_3. An additional coincidence in S_0 was required to keep accidentals to a very low rate. Counter S_0 and the transmission counters S_1, S_2, and S_3 consisted of discs of plastic scintillator 1/2-in. thick, viewed edgewise through lucite light pipes by RCA type 6810A phototubes. The phototubes were carefully shielded against stray magnetic fields. These counters ranged in diameter from 4.5 to 12 inches. Each was tested for uniformity of response over its entire area with a beta source. By suitable treatment of the internal reflecting surfaces of the counters, it was possible to reduce the variations in pulse height to less than $\pm 15\%$ between different parts of the counter. To ensure an efficiency near 100%, all counters were operated at voltages such that coincident pulses were about twice as large as required to drive the coincidence circuits to saturation.

D. Electronics

Conventional electronic techniques were employed. The coincidence circuits were of the type described by Wenzel;[4] with the clipping lines used, the resolving time was about 6×10^{-9} sec. The output of the monitor coincidence circuits was used to drive a discriminator-amplifier that provided a shaped pulse used as an input to a second coincidence circuit where a coincidence with S_0 and S_1 (for example) was required. Hewlett-

Packard Type 520A prescalers followed by conventional 1000 scalers were employed. These prescalers are capable of counting up to 10^7 pulses/sec. Our instantaneous counting rates ranged from 10^5/sec to 10^2/sec, depending on the beam energy.

Several extra coincidence units and scalers were used to monitor various types of accidentals. Generally these were quite low. In particular, the accidental rate in the Cerenkov counter never exceeded 2% of the counting rate for pions.

E. The Hydrogen Target and Other Absorbers Used.

The liquid hydrogen target used consisted of a 48-in.-long Mylar vessel 4-in. in diameter. Liquid hydrogen was supplied by gravity feed from a large reservoir directly above the target vessel. Both reservoir and target vessel were surrounded by a heat shield at liquid nitrogen temperature and enclosed in a vacuum. The construction of the target is described in detail in Ref. 5.

The density of liquid hydrogen at its normal boiling point is 0.0710 g/cm^3, from data in Ref. 6. From this should be subtracted the density of hydrogen gas in the empty target. The temperature of the gas was assumed to be that of the liquid, 20.3° K. The density of hydrogen gas at this temperature is 0.0013 g/cm^3.[6]

The other absorbers used were machined blocks of beryllium, graphite, aluminum, and copper, whose purity exceeded 99%. The thicknesses of the absorbers (listed in Table II) were chosen so that multiple Coulomb scattering corrections would be small for the smallest angles at which measurements were planned.

III. TREATMENT OF DATA: CORRECTIONS

A. Calculation of Cross Sections and Statistical Errors

The apparent cross section $\sigma(\theta)$ for a given geometry was calculated from

$$\sigma = -(1/nx) \log \left[(S/M)_F/(S/M)_E\right] , \qquad (2)$$

where $(S/M)_F$ and $(S/M)_E$ represent the ratios of surviving pions (or protons) to monitor counts with target full or target empty, respectively. The numbers of monitor counts and of surviving pions both were corrected for accidentals where necessary. As mentioned previously, these corrections were quite small.

The standard deviation in σ is given by

$$\Delta\sigma = (1/nx) \left[1/S_F - 1/M_F + 1/S_E - 1/M_E\right]^{1/2} . \qquad (3)$$

The statistical errors in the cross sections were generally approximately 1%. Statistical analysis of the reproducibility of repeated runs showed a small fluctuation outside of that expected from counting statistics. The probable error in a single measurement was found to be $\pm$ 1.4% in addition to the statistical error.

B. Corrections for Multiple Coulomb Scattering

When the angle subtended by the transmission counter is made small, the observed cross sections rise sharply because of the loss of particles by multiple Coulomb scattering in the absorber. Where necessary, corrections were applied to the data by using the method described by R. M. Sternheimer.[7] He assumes that the Coulomb scattering has a Gaussian distribution in angle with an rms space angle

$$\theta_{rms} = (E_S/\beta pc) \sqrt{L/L_{rad}} , \qquad (4)$$

where E_S = 21 Mev, p and βc are the momentum and velocity, respectively, and L/L_{rad} is the thickness of the absorber in radiation lengths. In attempting to correct the experimental points most affected by Coulomb scattering, we found that if this value of θ_{rms} was used the corrections were too large - the corrected values of $\sigma(\theta)$ fell well below the trend established by the points at large θ where no corrections were necessary. We found that the value of θ_{rms} from Eq. (4) had to be reduced by 30% to obtain good over-all agreement.[8]

Even with this modification the results were not always completely satisfactory, so that these corrections were assigned an error of $\pm$ 25% or more, depending on how well the beam distribution at the transmission counters was known. These corrections were important only in the low-energy hydrogen data when the solid angle subtended by the transmission counter was small. It was found that no corrections were necessary to the heavy-element data at any angles at which measurements were made. Furthermore, the effect of the large error assigned to the Coulomb scattering corrections to the hydrogen data was to minimize the statistical weight of the small-angle points, so that the latter had little effect on the extrapolated total cross sections (see next section).

C. Extrapolation of the Hydrogen Data to Obtain the Total Cross Section

For hydrogen, only the total cross sections for nuclear scattering were to be measured. To obtain an accurate value it is desirable that the solid angle subtended by the transmission counter be as small as possible, so that nearly all the particles undergoing nuclear scattering are removed from the beam. An effective lower limit is set by multiple Coulomb scattering at small angles, however; so in practice a small correction must be applied to the measured cross sections because of the nonzero solid angle

subtended by the counter. This was done by taking measurements at several solid angles and extrapolating the measured cross sections to zero solid angle. A linear dependence on solid angle was assumed. From the discussion in Sec. II-A, the slope of the extrapolation is $(d\sigma/d\Omega)_{el}$ plus a contribution due to the detection of charged secondaries. Neither term is expected to vary significantly over the range of angles involved (0 to 2 deg).

Data were taken at six solid angles ranging from 0.6×10^{-3} to 4.2×10^{-3} sr as measured from the center of the hydrogen. After corrections for multiple Coulomb scattering were made, no significant deviation from the expected linear dependence on solid angle was observed. The extrapolation yielded total cross sections about 2% higher than the experimental points at intermediate solid angles.

D. Contamination in the Beam

1. Contamination in the Pion Beam

The gas Cerenkov counter provided a very useful means for determining muon and electron contamination in the beam. If the gas pressure in the counter is raised gradually from a low value, first the electrons begin to count, then the muons, and later the pions. In this case, because of the small difference in velocities, it was possible to separate the muons and pions only at the lower energies. Figure 3 show the ratio of $M_1M_2CM_3$ coincidences to $M_1M_2M_3$ coincidences plotted against the index of refraction of the gas in the counter, for a beam momentum of 1.8-Bev/c. The threshold for 1.8-Bev/c muons and pions is also indicated. It is apparent that the muon contamination is small, probably less than 1% of the number of pions. The tail on the curve at low indices of refraction is presumably due to electrons.

a. Calculation of the muon contamination.

A curve such as in Fig. 3 indicates only the fraction of muons formed before the last bending magnet and thus having approximately the same momentum as the pions. Muons formed after the last bending magnet have a large spread in momentum and so do not cause a sharp rise in the index-of-refraction curve. For this reason, the total muon contamination in the beam at each energy was determined by calculation. To do this, the beam line was broken up into segments. The probability that a pion will decay between points X_1 and X_2 is given by

$$N(X_1) - N(X_2) = N_0 \left[\exp(-X_1/\lambda) - \exp(-X_2/\lambda)\right] , \qquad (5)$$

where $\lambda = \beta \gamma c \tau_0$ is the mean life in centimeters. It was then necessary to determine the probability that the muon would come off in such a direction that it would pass through the counter system. The contributions of all segments were then summed to get the fraction of muons in the beam.

Because of the complication caused by the Bevatron's magnetic field and the quadrupole, it was possible to calculate the contribution from the region before the last bending magnet only approximately. However, it was found that the total yield from this region was less than 0.2%. This low-yield figure is supported by the Cerenkov counter curve.

The calculation for the region following the last bending magnet was much simpler. Because there is no momentum selection, it is only necessary to calculate the solid angle subtended by the "limiting aperture" of the system (either M_3 or the transmission counter). This solid angle is then transformed into the c.m. system of the decaying pion. Since the decay is isotropic in this system, the probability of the muons' passing through the counters is just $1/4\pi$ times this solid angle. The only important

simplification in these calculations was to neglect the finite diameter of the beam. The maximum correction in the pion cross sections was 2%, which justifies such a simplification.

b. Calculation of the electron contamination.

Another contaminant in the pion beam at low energies was electrons. From Fig. 3 we can estimate their number at about 3% of the number of pions at 1.8 Bev/c, the energy at which the Cerenkov counter pressure curve was taken. No measurements were made at other momenta because of limitations on running time.

The major source of these electrons is the decay of π^0 mesons produced in the Bevatron target. These mesons decay almost immediately into two gamma rays, either of which can in turn produce an electron pair in the target material. The probability of producing a pair is roughly proportional to the available path length L in the target material.

It was possible to calculate the electron contamination in the beam at each momentum by using theoretical estimates of the yield of pions produced in the Bevatron target.[9] Briefly, the theoretical curves for π^0 production were used to estimate the spectrum of high-energy gamma rays. This was in turn used to calculate the electron yield from pair production relative to that of positive pions. The average path length $\bar{L}$ was calculated by using theoretical curves for the distribution of the proton flux striking the target.[10] The contribution of Dalitz pairs, estimated to be several percent of the total electron yield, was neglected.

The calculated values of the electron contamination ranged from 0 to 3% of the pion flux. For the conditions under which the Cerenkov counter curve (Fig. 3) was taken, the electron contamination was calculated to be 2.7%, in good agreement with the value of 3% estimated from Fig. 3.

An uncertainty of ±50% was assigned to the calculated values.

2. Contamination in the Proton Beam

Any beam particle that did not count in the Cerenkov counter was classed as a "proton." This would include K^+ mesons and heavier particles. Data of Burrowes et al. at 1.75 Bev/c indicate a yield of approximately six K^+ mesons per 10^{10} protons incident on their target, with a momentum acceptance of ±2%, and an estimated solid angle of 0.5×10^{-3} sr.[11] Comparing this value with the proton yields observed at 1.73 Bev/c in this experiment, one obtains a ratio $>10^3$ protons per K^+. This ratio can be expected to be still larger at higher energies.

If the gas Cerenkov counter and the associated anticoincidence circuits were not 100% efficient in removing pions from the proton channels, the result would be an effective pion contamination in the "proton beam." No experimental means of checking this was available, though the flatness of the index-of-refraction curve (Fig. 3) at high indices indicates that this counter is nearly 100% efficient when operated in coincidence. The efficiency in anticoincidence was therefore assumed to be $100\%\ ^{+0\%}_{-5\%}$, and the errors in the proton total cross sections increased correspondingly.

E. A Summary of the Sources of Error Considered in Assigning Errors to the Cross Sections

The following sources of error were taken into account in assigning errors to the total cross sections. All errors were combined in quadrature.

(a) Statistical errors in the measurements were considered. These were generally quite small (≈ 1%). The quoted errors also include the fluctuation outside of statistics which was observed in the data.

(b) At each energy and solid angle all the runs were averaged and the errors combined. The cross sections were then corrected for multiple Coulomb scattering, and the uncertainty in this correction was

combined with the other errors.

(c) The uncertainty in the extrapolation to zero solid angle was taken to be equal to the uncertainty in slope multiplied by the average solid angle.

(d) The final error in the pion cross section also includes the uncertainty in the electron contamination in the beam. Errors introduced by the uncertainty in the muon contamination in the pion beam and K^+ contamination in the proton beam were considered negligible.

(e) Errors in the proton total cross sections also include the uncertainty in the efficiency of the gas Cerenkov counter and associated electronics, as described in the previous section.

Errors in the heavy-nuclei cross sections include only statistical errors, and errors due to the fluctuations outside of statistics, as described above. Systematic errors that raise or lower all the data points together are not included in the quoted errors. These are thought to be $\lesssim 2\%$.

IV. EXPERIMENTAL RESULTS

A. Total Cross Sections for Positive Pions and Protons on Hydrogen in the Momentum Range 1.4 to 4.0 Bev/c

The measured π^+-p and p-p total cross sections are listed in Table I, and plotted in Fig. 4 as a function of beam momentum. Smooth curves have been drawn to show the gross features of the momentum dependence. Results from other experimenters are also shown for comparison.[12] In general, the agreement is good in regions where an overlap occurs.

Table I. Total π^+,p and p,p cross sections.

Momentum (Bev/c)	$\sigma(\pi^+,p)$ (mb)	$\sigma(p,p)$ (mb)
1.42	39.5 ± 0.50	$46.2 \begin{smallmatrix} + 0.5 \\ - 0.45 \end{smallmatrix}$
1.60	36.5 ± 0.97	$47.5 \begin{smallmatrix} + 1.02 \\ - 0.61 \end{smallmatrix}$
1.73	30.3 ± 0.42	$46.2 \begin{smallmatrix} + 0.82 \\ - 0.46 \end{smallmatrix}$
1.89	29.0 ± 0.75	$46.8 \begin{smallmatrix} + 1.51 \\ - 0.68 \end{smallmatrix}$
2.05	28.3 ± 0.63	$45.3 \begin{smallmatrix} + 1.12 \\ - 0.47 \end{smallmatrix}$
2.47	29.2 ± 0.57	$45.1 \begin{smallmatrix} + 0.83 \\ - 0.45 \end{smallmatrix}$
2.97	29.5 ± 0.53	$44.5 \begin{smallmatrix} + 0.46 \\ - 0.42 \end{smallmatrix}$
3.58	28.6 ± 0.46	43.2 ± 0.43
4.00	27.8 ± 0.53	41.6 ± 0.62

B. Cross Sections for Positive Pions and Protons on Be, C, Al, and Cu at 3.0 Bev/c

The measured cross sections for 3.0-Bev/c pions and protons are given in Table II as a function of $\Delta\Omega$, the solid angle subtended by the transmission counter as seen from the center of the absorber. The estimated errors are also indicated. The minimum values of $\Delta\Omega$ were such that corrections for multiple Coulomb scattering were still negligible, and the maximum values were such that most of the diffraction scattering was included in the cone subtended by the counter.

Some of the beryllium measurements were made with two different absorber thicknesses as a check on the method. The results are listed separately in Table II, but the two sets of measurements were combined when the data were fitted.

The pion cross sections have been corrected for muon and electron contamination as described in Sec. III-D. The method used to obtain total and absorption cross sections from the heavy-nuclei data is discussed in Sec. VI-B.

Table II. Heavy-element cross sections at 3.0 Bev/c

Run	$\Delta\Omega$ (msterad)	π^+ σ (mb)	π^+ $\Delta\sigma$ (mb)	p σ (mb)	p $\Delta\sigma$ (mb)
		Beryllium (16.5 g/cm^2)			
1	1.64	226.9	4.40	283.3	1.82
1	3.09	215.7	3.90	265.3	1.64
1	3.91	209.0	3.30	258.3	1.61
2	5.26	197.5	5.96	252.4	1.62
2	10.47	180.3	6.45	224.4	1.47
2	14.11	167.5	5.59	212.4	1.38
3	11.54	178.0	1.97	221.2	1.52
3	24.5	154.7	2.01	186.3	1.50
3	35.6	141.6	1.61	171.9	1.48
		Beryllium (8.24 g/cm^2)			
1	5.26	199.9	4.88	252.9	4.70
1	10.47	181.2	4.54	223.5	5.58
1	14.11	171.9	4.53	211.8	4.48
		Carbon (17.1 g/cm^2)			
1	1.64	267.9	3.85	341.2	2.66
1	3.09	247.4	4.10	312.4	3.50
1	3.91	235.7	3.60	302.0	3.18
2	5.26	237.7	2.78	297.7	2.24
2	10.47	210.0	2.00	257.5	1.82
2	14.11	195.1	2.78	242.8	1.63
3	11.54	216.7	7.25	265.0	6.30
3	24.5	193.9	12.5	224.9	5.80
3	35.6	176.2	6.73	210.9	4.50
		Aluminum (12.0 g/cm^2)			
1	1.49	542.	12.2	658.	7.6
1	2.80	488.	14.7	582.	8.4
1	3.92	447.	12.2	542.	6.9
2	5.61	439.	14.0	504.	6.8
2	11.39	386.	17.4	431.	8.8
2	19.5	355.	14.6	400.	6.3
		Copper (6.80 g/cm^2)			
1	1.49	1009.	34.3	1209.	10.0
1	2.80	832.	36.6	986.	9.9
1	3.52	772.	34.7	947.	8.6
2	2.29	900.	27.0	1091.	8.8
2	4.41	724.	34.2	909.	13.8
2	5.66	716.	26.1	881.	7.8

V. OPTICAL MODEL ANALYSIS OF THE NUCLEAR CROSS SECTIONS

A. Introduction

By "optical model" we mean that model in which the nucleus is represented by a potential well. This potential may have both a real and an imaginary part as well as spin-orbit terms, though the latter are not considered here. With this description, the many-body problem of a particle scattering on a nucleus is replaced by a soluble two-body interaction. Much theoretical work along these lines has been directed toward calculating these potentials, starting with a knowledge of the more fundamental interaction with individual nucleons. An early result was a relation between the nuclear potential integrated over the volume of the nucleus, and the amplitude for scattering by free nucleons. With reasonable assumptions concerning the extent and shape of the nuclear potential, we were able to compare the optical-model predictions with our experimental results. The method used and the results will be discussed in this section. In Part B the relation between the integrated optical potential and the amplitude for scattering by free nucleons is given, and the integrated potentials are calculated for 3.0-Bev/c pions and protons. Part C describes how optical potentials yielding cross sections that best fit the experimental data were obtained. Because it is impossible to calculate the best-fit potentials directly from the experimental cross sections without using questionable approximations, it was necessary to first "guess" a potential and then calculate cross sections that were in turn compared with the experimental values. The cross sections were calculated by an essentially exact solution of the relativistic Schrödinger equation. In Part D we present the best-fit potentials and compare them with the predicted values obtained in Part B.

B. Calculation of the Integrated Optical Potentials from the Interaction with Free Nucleons

1. General

For a given particle incident on a nucleus, it can be shown that the optical potential integrated over the nuclear volume is proportional to the forward amplitude for scattering by free nucleons (as averaged over all the nucleons in the nucleus).[13,14] The relation is

$$\frac{1}{A}\int W^{(1)}(\vec{r})\, d^3r = -\frac{2\pi\hbar^2}{M}\,\frac{E_T^*}{E_0}\left[\frac{Z}{A} f_p(0) + \left(1 - \frac{Z}{A}\right) f_n(0)\right], \quad (6)$$

where $W^{(1)}(\vec{r})$ is the first-order optical potential at a point $\vec{r}$ in the nucleus, E_0 the total energy of the incident pion (or proton) in the laboratory system, E_T^* the total energy in the pion-nucleon (or proton-nucleon) c.m. system, and M the nucleon mass; $f_p(0)$ and $f_n(0)$ are the c.m. forward scattering amplitudes for scattering by free protons and free neutrons, respectively.

Equation (6) must be corrected to take into account the effects of the Pauli exclusion principle, which can raise or lower the effective potentials depending on the energy of the incident particle. At low energies it acts to inhibit collisions with small momentum transfers, thus decreasing the potentials (in absolute value). At high energies this effect is small and is overshadowed by another that tends to increase the optical potentials. The latter effect is the mutual repulsion of nucleons at small distances, which keeps them apart and makes them more effective as scattering targets. At 3.0 Bev/c the over-all effect is an increase in the potentials of approximately 15%.

For small nuclei, Eq. (6) must be further corrected for terms of order 1/A which appear in a more careful derivation. These terms do not appear in the Born approximation, and we shall hopefully neglect them. We

shall also neglect a correction to the pion-nucleus potentials due to the possibility of direct absorption by two or more nucleons in the nucleus in reactions of the type $\pi^+ + p + n \rightarrow p + p$. These reactions are important at low energies, but are not expected to play a significant role at 3.0 Bev/c. Corrections to the proton-nucleus potentials due to the identity of the incident and target particles are also expected to be small.[15]

2. Calculation of Potentials for Pion-Nucleus Scattering

For positive pions, we have $f_p \equiv f(\pi^+,p)$, and $f_n \equiv f(\pi^+,n) = f(\pi^-,p)$ by charge symmetry. Cronin has used the total cross sections of this and other experiments to calculate from dispersion relations the real parts of the forward scattering amplitudes for pion scattering.[16] Extrapolating his results slightly to 3.0 Bev/c, and transforming to the c.m. system, we have

$$\mathcal{R}e\left[f(\pi^+,p)\right] = -0.095; \quad \mathcal{R}e\left[f(\pi^-,p)\right] = -0.26 \text{ fermi}.$$

Using $\sigma_T(\pi^+,p) = \sigma_T(\pi^-,p) = 2.9$ fermi^2, we have

$$\mathcal{I}m\left[f(\pi^+,p)\right] = \mathcal{I}m\left[f(\pi^-,p)\right] = \frac{k}{4\pi}\,\sigma_T = 1.29 \text{ fermi}.$$

This yields for $Z/A \simeq 1/2$ the first-order potential

$$\frac{1}{A}\int W^{(1)}(r)\, d^3r = (39.5 - 286\, i) \text{ Mev-fermi}^3. \qquad (7)$$

The real part of the potential is therefore small and repulsive.

The first-order potentials must be corrected for nuclear correlation brought about by the effects of the exclusion principle. According to Watson and Zemach,[17] the optical potential correct to second order is

$$W^{(2)} = \left\langle U^{(1)} - i\left|V^{(1)}\right|\right\rangle \quad (1 + i\,\Delta_R + \Delta_I), \qquad (8)$$

where $U^{(1)} - i\left|V^{(1)}\right|$ is the first-order potential. For $\beta \approx 1$ we have

$$\Delta_R = -\frac{U^{(1)}_R}{\hbar c}c \; ; \quad \Delta_I = -\frac{V^{(1)}_R}{\hbar c}c \tag{9}$$

The correlation length R_c is a measure of the correlation of nucleon positions in the nucleus. Its value can be calculated for particular models of the nucleus. For a degenerate Fermi gas model, $R_c \approx -0.4$ fermi.[17] (Negative values of R_c correspond to an over-all repulsive interaction.) Using the Brueckner model, we get $R_c \approx -0.63$ fermi.[18] We shall use the latter value. From Eq. (7), assuming a square-well potential of radius $1.2\,A^{1/3}$, we find $U^{(1)} = +5.5$, $\left|V^{(1)}\right| = 39.5$. This yields $\Delta_R = -0.02$ and $\Delta_I = +0.125$, and the integrated optical potential for pions, correct to second order, is

$$\frac{1}{A}\int W^{(2)}(\vec{r})d^3r = (38.8 - 323i)\ \text{Mev-fermi}^3. \tag{10}$$

3. Calculation of the Proton-Nucleus Optical Potentials

For p-p and p-n scattering, little is known about the real part of the forward scattering amplitudes at high energies. The most accurate data seem to be those of Preston, Wilson, and Street,[19] who find, at 3.8 Bev/c,

$$\left|\mathrm{Re}\left[f(p,p)\right]\right| \leq 0.1 \cdot \left|\mathrm{Im}\left[f(p,p)\right]\right|.$$

No data are available yet on $\mathrm{Re}\left[f(p,n)\right]$. We therefore assume, for both p-p and p-n scattering, $|\mathrm{Re}f| \ll |\mathrm{Im}f|$, so that for proton scattering the real part of the optical potential is small compared with the imaginary part. Since the fits to the experimental data are quite insensitive to the real potential when it is small, the above assumption is sufficient for our purposes.

Using $\sigma_T(p,p) = 44.5$ mb at 3.0 Bev/c (from Table I), and

$\sigma_T(n,p) = 41.5$ mb,[20] we obtain, from Eq. (6),

$$\frac{1}{A}\int V^{(1)}(\vec{r})d^3r = -400 \text{ Mev - fermi}^3, \tag{11}$$

for $Z = A/2$.

If we assume that Eqs. (8) and (9) for the second-order potential are correct for protons as well as pions, then neglecting Δ_R we have

$$\frac{1}{A}\int V^{(2)}(\vec{r})d^3r = -470 \text{ Mev-fermi}^3.$$

C. The Method Used in Fitting the Experimental Data

1. The Shape of the Potential Well

In fitting the experimental data a process of trial and error was used. A potential well was chosen, and cross sections calculated. These cross sections were compared with the experimental ones, and the process repeated until good fits were obtained.

In this method it is necessary to assume a shape for the nuclear potential well. In the past, a square-well potential was usually chosen to simplify calculations. This shape, however, is quite unrealistic and usually leads to unsatisfactory agreement with experiment.[21] Data from electron-scattering experiments are consistent with a nuclear density distribution having a Fermi shape.[22] Since the shape of the optical potential is expected to resemble that of the nuclear density distribution, a Fermi well was used in fitting the data of this experiment. It was further assumed that both the real and imaginary parts of the potential have the same shape. The potential $W(r)$ therefore has the form

$$W(r) = U(r) + i\,V(r) = \frac{U_0 + i\,V_0}{1 + e^{(r-r_0)/a}}, \tag{12}$$

where r_0 is the radius at which the potential drops to $(U_0 + i\,V_0)/2$ and a is a parameter determining the rate of fall-off. For $a \ll r_0$,

the well is almost "square."

In the initial attempts to fit the data, it became apparent that good fits could be obtained over a wide range of values of the parameters U_0, V_0, r_0, and a, if all were allowed to vary. Increasing r_0 could be compensated for by decreasing U_0 and V_0; decreasing a could be compensated by decreasing U_0 with respect to V_0. It was therefore decided to fix r_0 and a at the values obtained in the electron-scattering experiments. The values used are listed in Table III, which also lists the values of U_0 and V_0 that yield the integrated potentials of Eqs. (10) and (11). The electron-scattering data for beryllium were fitted with a modified exponential density distribution;[22] however, it was found that this could be well approximated by a Fermi distribution with a suitable choice of r_0 and a. Figure 5 shows $U(r)/U_0$ for the potential distributions used in fitting the data. The modified exponential shape used in fitting the beryllium electron-scattering data is also shown. Note that for beryllium $U(r)$ must be multiplied by $(0.62)^{-1}$ to normalize $U(r)/U_0$ to unity at the origin.

2. The Computer Program Used in Calculating the Optical-Model Cross Sections

The program used to calculate the cross sections is a modification of that described by Bjorklund, Blandford, and Fernbach.[23] The original version of this program solves the Schrödinger equation for a complex nuclear potential plus a Coulomb potential corresponding to a nucleus with a uniform charge distribution of radius r_0:

$$U_{Coul} = \frac{Ze^2}{2r_0}\left[3 - \left(\frac{r}{r_0}\right)^2\right] \quad \text{for } r < r_0, \tag{13}$$

$$U_{Coul} = \frac{Ze^2}{r} \quad \text{for } r > r_0 .$$

Table III. Well parameters and predicted potentials.

Nucleus	r_o	a	$\langle r^2 \rangle^{1/2}$	Pions		Protons	
				U_0(Mev)	V_0(Mev)	U_0(Mev)	V_0(Mev)
Be	0.429	0.84	3.03	16.5	-137.6	≈0	-200
C	2.25	0.45	2.41	7.0	-58.1	≈0	- 85
Al	3.01	0.60	3.22	6.6	-54.9	≈0	- 80
Cu	4.26	0.53	3.84	6.6	-54.9	≈0	- 80

The resulting wave equation must be integrated numerically for each angular momentum state. The complex phase shifts are then determined by matching the resulting wave functions to Coulomb wave functions at the edge of the nucleus. The differential cross sections for scattering at any angle and the total inelastic cross sections can then be calculated.

The original version was modified to treat relativistic particles as follows:

(a) The original program solved the radial Schrödinger equation,

$$\left[-\frac{1}{r^2}\frac{d}{dr}\left(r^2\frac{d}{dr}\right) + \frac{\ell(\ell+1)}{r^2} \right] R = 2m \left[T - W(r) \right] R. \qquad (14)$$

It was assumed that the scattering of both pions and protons could be described by the Klein-Gordon equation,[24]

$$\left[-\frac{1}{r^2}\frac{d}{dr}\left(r^2\frac{d}{dr}\right) + \frac{\ell(\ell+1)}{r^2} \right] R = \left[(E - W(r))^2 - m^2 \right] R. \qquad (15)$$

Actually, the Dirac equation is the proper wave equation for protons; however, if spin effects are neglected, the Dirac equation reduces to the Klein-Gordon equation.[25] Neglecting terms in $(W/E)^2$ compared to unity, we can rewrite Eq. (15) as

$$\left[-\frac{1}{r^2}\frac{d}{dr}\left(r^2\frac{d}{dr}\right) + \frac{\ell(\ell+1)}{r^2} \right] R = \left[p^2 - 2EW(r) \right] R, \qquad (16)$$

where $p^2 = E^2 - m^2$. Equation (16) has the same form as Eq. (14) with $2mT$ replaced by p^2 and m replaced by E.

(b) The original version had to be modified to treat problems in which angular momentum states with $\ell = 100$ were important. The relativistic version allows $\ell_{max} \leq 200$. Running time for the 3.0-Bev/c problems was 10 to 20 minutes.

As a check on the new version, another program was written independently to calculate the scattering by a real "square well" using

analytical solutions. A comparison of the two programs for 3.0-Bev/c pions showed agreement to approx 0.2%, when the fall-off parameter a was made small in the Fermi-well case to approximate a square well.

3. Method Used in Comparing the Calculated Cross Sections with the Experimental Data

If we neglect the finite angular resolution of the counter telescope, it is expected that the measured cross section $\sigma(\theta)$ will have the following dependence on the angle θ subtended by the edge of the transmission counter:[26]

$$\sigma(\theta) = \int_{\theta'=\theta}^{\theta'=\pi} \frac{d\sigma_{el}(\theta')}{d\Omega'} \, d\Omega' + \sigma_a - 2\pi\,\eta\,(1-\cos\theta) \qquad (17)$$

The first term is the cross section for elastic scattering at angles greater than θ; the second represents the loss of particles due to all inelastic processes (absorption). The third term results from inelastic events that give rise to charged secondary particles that count in the transmission counter and so lower the apparent cross section. We assume that for angles at which measurements were made ($0 < \theta < 6$ deg) the differential cross section for producing charged secondaries, η, is approximately constant, so that this term is proportional to the solid angle subtended by the transmission counter, $2\pi(1 - \cos\theta)$. The proportionality constant η can be determined for each pair of U_0 and V_0 by a least-squares fit to the data, with the restriction that η be positive.

If the finite angular resolution of the counter system is taken into account, Eq. (17) must be replaced by

$$\sigma(\theta) = \int_0^{\pi} \frac{d\sigma_{el}(\theta')}{d\Omega'} \, \mathcal{R}(\theta,\theta') \, d\Omega' + \sigma_a - 2\pi\,\eta\,(1 - \cos\theta), \qquad (18)$$

where $\mathcal{R}(\theta,\theta')$ is the probability that a particle scattered at an angle

θ' will miss the transmission counter. $\mathcal{R}(\theta,\theta')$ was calculated for each value of θ and θ', by using the measured distributions of beam particles at the transmission counters.

In fitting the experimental data to the functional form given in Eq. (18), all calculations were carried out in the c.m. system of the incident particle and the target nucleus. This merely involved transforming the angle θ to its corresponding angle θ^* in the c.m. system.

For each pair of U_0 and V_0, a value of χ^2 was determined, where

$$\chi^2 = \sum_{i=1}^{N} \left[\frac{\sigma^i_{meas} - \sigma^i_{calc}}{\Delta\sigma_{meas}} \right]^2 . \qquad (19)$$

For a "good fit," χ^2 is approximately equal to the number of experimental points minus the number of fitted parameters.

D. The Results of the Analysis: Comparison of the Best-Fit Potentials with the Predicted Ones

Figures 6 and 7 show plots of χ^2 vs V_0 for $U_0 = 0$ as theory predicts. $V(r = 0) = 0.62\ V_0$ has been plotted for beryllium for easier comparison with the other nuclei studied. Considering the uncertainty in the predicted values, the best-fit values of V_0 are generally in good agreement with the predicted ones. The predicted potentials seem to be slightly low in the case of pion-nucleus scattering. There also seems to be a substantial disagreement between the predicted potentials and the best-fit values for both pions and protons incident on copper. This is as yet unexplained.

If U_0 is kept fixed, the minimum values of χ^2 are expected to be about 7 for Be and C, and about 4 for Al and Cu, corresponding to the two fitted parameters V_0 and η. The values obtained were generally somewhat larger. The explanation for this is discussed below.

The variation of χ^2 with U_0 was also studied. Figure 8 shows a plot of χ^2 vs U_0 for positive pions scattered by Be, C, Al, and Cu nuclei. For each value of U_0 the imaginary potential V_0 was adjusted to give a minimum in χ^2. It can be seen that the fits are improved somewhat if U_0 is made approximately equal to V_0 in absolute value. The predicted values of U_0 from Table III are indicated by arrows. As mentioned previously, the fits are not sensitive to U_0 when U_0 is small. Results for the case of incident protons are quite similar. When U_0 was allowed to vary, the minimum values of χ^2 tended to be smaller than might be expected statistically. This is probably due to a slight overestimation of the experimental errors.

It is apparent from Fig. 8 that except for beryllium the large values of U_0 are only slightly favored statistically over the predicted ones. The magnitude of this discrepancy is further illustrated in Fig. 9 which compares the experimental cross sections for pions on beryllium with the calculated ones for $U_0 = 0$ (the predicted value), and also for the best-fit value of U_0. Even in this case, where the high values of U_0 are most favored statistically, the discrepancy could be removed completely if the experimental cross sections at intermediate angles were raised approximately 2%, or if the small-angle points were lowered about the same amount (this latter alternative would also involve readjusting the best-fit values of V_0 and η).

It is therefore quite possible that this discrepancy arises from a small systematic error in the cross-section measurements, or to some deficiency in the method used in fitting the data. Possible explanations are discussed in detail below.

VI. DISCUSSION OF RESULTS

A. The Total Cross Sections for Scattering by Hydrogen

A striking aspect of the π^+-p total cross section plotted in Fig. 4

is its near constancy above 2 Bev/c. This is interesting in view of a theorem due to Pomeranchuk stating that if the total cross sections for a particle and its antiparticle on hydrogen approach constant values at high energies, these limits must be equal.[27] The available data for π^--p scattering show a similar flattening at high energies at approximately the same value.[12b] This is the best experimental evidence to date for the validity of Pomeranchuk's theorem.

The p-p cross sections in the momentum range of this experiment show no sign of approaching a constant value. At 4.0 Bev/c the $\bar{p}$-p cross section is still 30 mb higher than the p-p cross section. Recent measurements at the CERN accelerator indicate that the difference decreases to 10 mb at 10.7 Bev/c.[12b]

B. Discussion of the Fitted Values of the Optical Potentials

The discrepancy between the best-fit experimental values of the real potential and the calculated ones is considerably outside the uncertainty in the calculated potentials. There are several possible explanations for this result.

(a) When the fall-off parameter a was made smaller, good fits were obtained with considerably lower real potentials. To obtain agreement with the predicted values of U_0, it was necessary to reduce a almost to zero. It is quite difficult, however, to reconcile this with current theories regarding the structure of the nucleus. The variation of the best-fit values of the real potential (integrated) with r_0 was also studied, and it was found that the fitted values were insensitive to small changes in r_0.

(b) The neglect of spin-orbit coupling might explain the discrepancy in the proton scattering results. Furthermore, since all the nuclei studied except carbon had nuclear spins,[28] the most general optical potential for both pions and protons includes a term proportional to $\vec{L} \cdot \vec{I}$, where $\vec{L}$ is

the angular momentum of the incident particle and $\vec{I}$ the nuclear spin. Both this and the spin-orbit term, however, would be of relative order 1/A, while the observed discrepancy does not seem to depend on A.

(c) In comparison of the experimental cross sections with the calculated ones as given by Eq. (18), it was assumed that η, the differential cross section for the production of charged secondaries, was constant over the range of angles studied. This assumption, though necessary, is open to question. Drell has in fact suggested that at high energies the production of secondary particles from inelastic collisions is strongly peaked forward at lab angles $\leq m/E_0$, where m is the pion mass and E_0 the total energy of the incident particle in the laboratory system.[29] At 3.0 Bev/c this characteristic angle is ≈ 3 deg. It can be seen from Fig. 9 that this effect need not be large to explain the observed discrepancy.

In view of the above discussion, and because the fits were found to be rather insensitive to U_0, we conclude that there is no real disagreement between the results of this experiment and the values of the real potential predicted from the optical model and dispersion relations. A definitive test could be made if the differential elastic cross sections were measured directly. For both pions and protons, the experimentally determined values of the imaginary optical potential are generally in quite good agreement with the predicted ones. There is possibly a disagreement in the case of scattering on copper.

Two quantities of considerable interest are the total nuclear cross section σ_T and the absorption cross section σ_a. For heavy nuclei, it is difficult to measure the total cross section at high energies because Rutherford scattering is large over the major part of the diffraction pattern. However, once optical-well parameters that fit the experimental data are

determined, it is possible to define the total nuclear cross section in terms of these. To do this, we simply "turn off" the Coulomb interaction and calculate the total cross section for the potential well with no Coulomb potential. For light nuclei this is the same as obtained by extrapolating the measured cross sections to 0 deg, as is usually done.

The absorption cross section can also be defined in terms of the best-fit parameters. The total elastic cross section σ_{el} is then $\sigma_T - \sigma_a$. The values of σ_a and σ_{el} thus obtained are listed in Table IV. The best-fit values of V_0 when U_0 is restricted to be small are also summarized there.

The errors in the values of V_0 given in Table IV are such that at the upper and lower limits χ^2 is three times the minimum value. The upper and lower limits on σ_a and σ_{el} are the values corresponding to the upper and lower limits on V_0.

For comparison with our results, Table IV also lists the values of σ_a and σ_{el} found by Wikner for the scattering of 4.3-Bev/c negative pions.[30] His results for σ_a are in good agreement with ours, but his values of σ_{el} are more than twice as large. Wikner's analysis with a square-well potential showed that his data indicated the real potential to be somewhat larger than the imaginary one. Our data, on the other hand, are consistent with a real potential $U_0 \approx 0$, if a square well is assumed.

If this apparent change in the total elastic cross sections were verified by subsequant experiments, it would constitute a violation of charge symmetry at high energies. The only alternative possible is that the real potential increases dramatically between 3.0 and 4.3 Bev/c. Since present data show that the total pion-nucleon cross sections are essentially constant in this energy range, this presumes a breakdown of the pion-nucleon dispersion relations. A check on Wikner's measurements with improved techniques now available will be necessary before any definite conclusion is possible.

Table IV. Pion-nucleus absorption and elastic cross sections

	This Experiment (3.0 Bev/c π^+)			Wikner (4.3 Bev/c π^-)	
	V_0 (Mev)	σ_a	σ_{el}	σ_a	σ_{el}
π + Be	154. $\pm$ 9.0	192 $\pm$ 8	41.5 $\pm$ 3.5	177 $\pm$ 9	125 $\pm$ 18
π + C	59.6 $\pm$ 4.0	213 $\pm$ 8	66.6 $\pm$ 7	219 $\pm$ 8	167 $\pm$ 22
π + Al	58.5 $\pm$ 4.1	428 $^{+15}_{-12}$	160 $^{+14}_{-12}$	470 $\pm$ 10	356 $\pm$ 41
π + Cu	69.0 $^{+13.5}_{-8.0}$	790 $^{+41}_{-26}$	445 $^{+60}_{-23}$	725 $\pm$ 25	895 $\pm$ 93
p + Be	109 $\pm$ 6	236 $\pm$ 4	64.8 $\pm$ 2.4		
p + C	84.3 $\pm$ 4.3	260 $\pm$ 6	107 $\pm$ 6		
p + Al	81.5 $\pm$ 6.5	503 $\pm$ 16	236 $\pm$ 17		
p + Cu	120 $\pm$ 24	914 $\pm$ 44	620 $\pm$ 65		

ACKNOWLEDGMENTS

The authors are happy to take this opportunity to thank the many people whose assistance made this work possible. We are particularly indebted to Dr. Victor Perez-Mendez for providing the hydrogen target and the gas Cerenkov counter, and for his invaluable help during the experiment. Special thanks are also due to Drs. Wilmot N. Hess and Thomas J. Devlin for their able assistance, and to Jerome Helland for his assuming much of the responsibility in the preparations for the experiment.

We are indebted to Professor Kenneth Watson for advice on the theoretical aspects of the experiment and to Ken Lou for his help in solving the many engineering problems associated with this experiment.

FOOTNOTES AND REFERENCES

*This work was done under the auspices of the U. S. Atomic Energy Commission.

†Submitted by one of the authors (M. J. L.) in partial satisfaction of the requirements for the degree of Doctor of Philosophy at the University of California, Berkeley, California.

1. The total π^+-p and p-p cross sections presented here were previously reported in Phys. Rev. Letters 3, 568 (1959). The values given here are slightly different because of a more thorough analysis of the data and a correction for electron contemination in the pion beam that was previously neglected. The $\pi^{\pm}$-p total cross sections at lower energies were measured with a different experimental arrangement and are presented in the preceding article ($\pi^{\pm}$-p Total Cross Sections in the Range 450 to 1650 Mev).
2. There is also a contribution to the slope due to charged secondary particles produced in inelastic collisions. As θ is increased, more of these strike the detector and the apparent cross section decreases.
3. J. H. Atkinson and V. Perez-Mendez, Rev. Sci. Instr. 30, 865 (1959).
4. William A. Wenzel, Millimicrosecond Coincidence Circuit, University of California Radiation Laboratory Report UCRL-8000, October 1957 (unpublished). The Lawrence Radiation Laboratory Counting Handbook, UCRL-3307 Rev., describes all the counting equipment used in this experiment.
5. D. D. Newhart, V. Perez-Mendez, and W. L. Pope, Liquid Hydrogen Target, Lawrence Radiation Laboratory Report UCRL-8857, August 1959 (unpublished).
6. Wooley, Scott, and Brickwedde, J. Research N.B.S. 41, 379 (1948).
7. R. M. Sternheimer, Rev. Sci. Instr. 25, 1070 (1954).

8. Barkas and Rosenfeld (in Data for Elementary-Particle Physics, Lawrence Radiation Laboratory Report UCRL-8030-Rev, April 1961, unpublished) suggest that the rms Coulomb scattering angle given by Eq. (4) should be reduced by 20% to agree with the Molière theory.

9. D. Morgan, Some Theoretical Estimates of the Yield of Secondary Particles Produced by 7-Gev Protons, Atomic Energy Research Establishment (Harwell) Report R3242, February 1960 (unpublished).

10. J. W. Burren, The Extraction System for Nimrod (Part I), Atomic Energy Research Establishment (Harwell) Report M521, November 1959.

11. Burrowes, Caldwell, Frisch, Hill, Ritson, and Schluter, Phys. Rev. Letters 2, 117 (1959).

12a. F. Chen, C. Leavitt, and A. Shapiro, Phys. Rev. 99, 857 (1955).

b. Von Dardel, Frisch, Mermod, Milburn, Piroué, Vivargent, Weber, and Winter, Phys. Rev. Letters 5, 333 (1960).

c. J. C. Brisson, J. Detoeuf, P. Falk-Vairant, Van Rossum, and G. Valladas, Nuovo cimento 19, 210 (1961).

d. Thomas J. Devlin, Burton J. Moyer, and Victor Perez-Mendez, preceding article. Preliminary data appear in Phys. Rev. Letters 4, 242 (1960).

13. R. Lipperheide and D. S. Saxon, Phys. Rev. 120, 1458 (1960).

14. R. M. Frank, J. L. Gammel, and K. M. Watson, Phys. Rev. 101, 891 (1956).

15. W. B. Riesenfeld and K. M. Watson, Phys. Rev. 102, 1157 (1956).

16. James W. Cronin, Phys. Rev. 118, 824 (1960).

17. K. M. Watson and C. Zemach, Nuovo cimento 10, 452 (1958).

18. T. K. Fowler and K. M. Watson, Nuclear Phys. 13, 549 (1959).

19. W. M. Preston, Richard Wilson, and J. C. Street, Phys. Rev. 118, 579 (1960).

20. John H. Atkinson, 5-Bev Neutron Cross Sections in Hydrogen and Other Elements (Ph.D. Thesis), Lawrence Radiation Laboratory Report UCRL-8966, November 1959 (unpublished).

21. Herman Feshbach, The Optical Model and Its Justification, Ann. Rev. Nuclear Sci. 8, 49 (1958).

22a. Robert Hofstadter, Revs. Modern Phys. 28, 214 (1956).

b. Robert Hofstadter, Ann. Rev. Nuclear Sci. 7, 231 (1957).

23. F. Bjorklund, I. Blandford, and S. Fernbach, Phys. Rev. 108, 795 (1957).

24. L. I. Schiff, Quantum Mechanics (McGraw-Hill Book Company, Inc., New York, 1955), Chap. 12.

25. K. Gatha and R. Riddell, Jr., Phys. Rev. 86, 1035 (1952).

26. This method of fitting the data is similar to that used by Cronin, Cool, and Abashian, Phys. Rev. 107, 1121 (1957).

27. I. Pomeranchuk, J. Exptl. Theoret. Phys. (U.S.S.R.) 34, 725 (1958). (Translation: Soviet Phys. - JETP 34 (7), 499 (1958).

28. Be^9 has spin I = 3/2, Al^{27} has spin I = 5/2, Cu^{63} and Cu^{65} have spin 3/2.

29. S. D. Drell, Phys. Rev. Letters 5, 342 (1960).

30. Frederick Wikner, Nuclear Cross Sections for 4.2-Bev Negative Pions (Ph.D. Thesis), University of California Radiation Laboratory Report UCRL-3639, January 1957 (unpublished).

FIGURE CAPTIONS

Fig. 1. Variation of cross section with subtended angle (schematic).

Fig. 2. Experimental arrangement. Magnetic shielding has been omitted for clarity.

Fig. 3. Cerenkov counter index-of-refraction curve at 1.8 Bev/c.

Fig. 4. Total π^+-p and p-p cross sections. Data of other experimenters (Ref. 12) are shown for comparison.

Fig. 5. Form factors for potential wells used in fitting data;

$$\rho(r) = \left[1 + e^{(r-r_0)/a}\right]^{-1} .$$

Fig. 6. χ^2 vs V_0 when $U_0 = 0$ for 3.0-Bev/c pions incident on several nuclei. $V(r = 0) = 0.62\ V_0$ has been plotted for Be for easier comparison with the other nuclei. The predicted values from Table III are

$|V(r = 0)| = 137.6 \times 0.62 = 85$ Mev for Be, and $|V_0| = 58.1$, 54.9, and 54.9 Mev for C, Al, and Cu, respectively.

Fig. 7. χ^2 vs V_0 when $U_0 = 0$ for 3.0-Bev/c protons incident on several nuclei. For easier comparison with the other nuclei, $V(r = 0) = 0.62\ V_0$ has been plotted for Be. The predicted values from Table III are $|V(r = 0)| = 200 \times 0.62 = 124$ Mev for Be, and $|V_0| = 85$, 80, and 80 Mev for C, Al, and Cu, respectively.

Fig. 8. The minimum values of χ^2/K for each U_0. K is the number of degrees of freedom in the fit (6 for Be and C, 3 for Al and Cu). For easier comparison with the other nuclei $U(r = 0) = 0.62\ U_0$ is plotted for Be.

Fig. 9. Examples of fits to the experimental data. $U_0 = 0$ is the predicted value of U_0; θ^* is the angle in the pion-nucleus center-of-mass system.

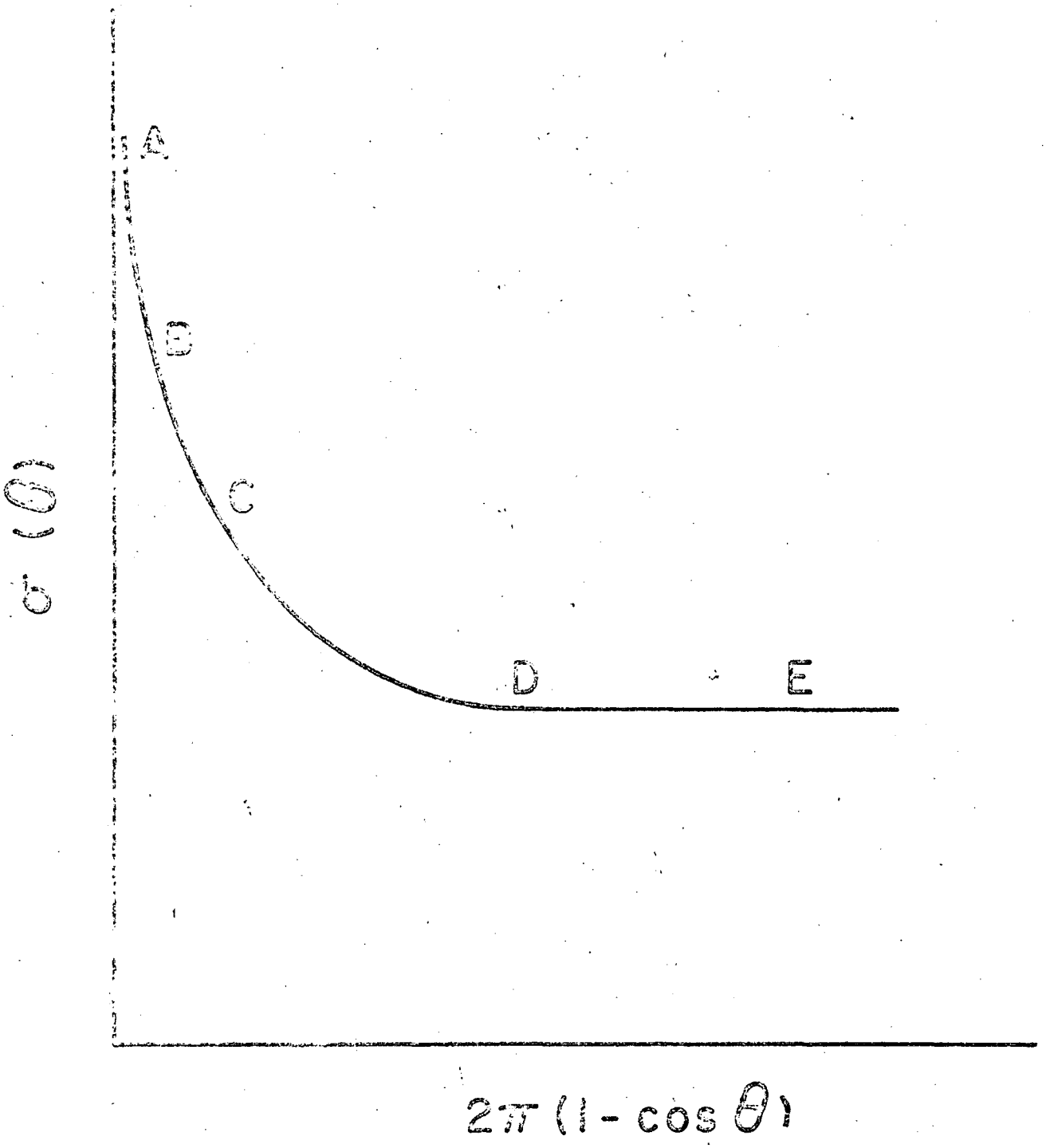

Fig 1

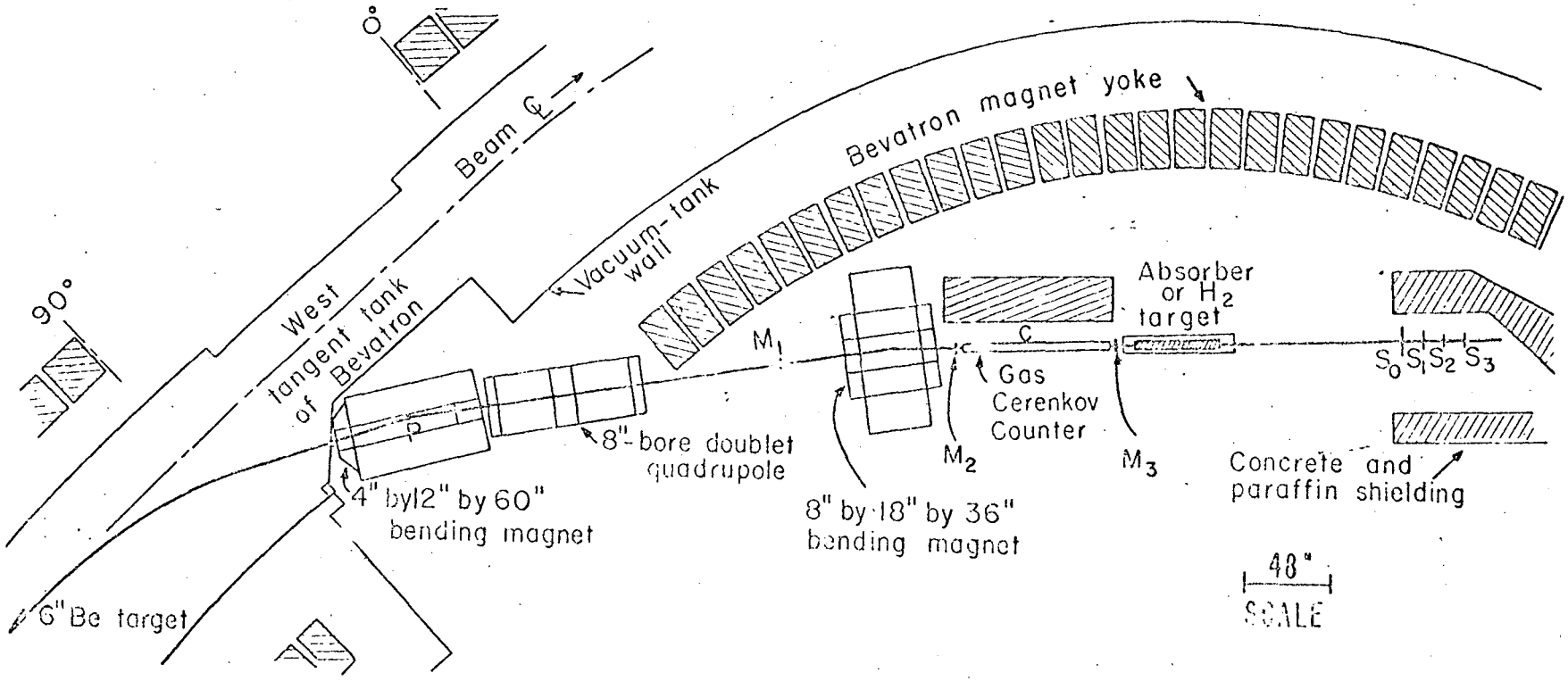
0°
Beam ℄
Bevatron magnet yoke
Vacuum-tank wall
West tangent tank of Bevatron
90°
M1
C
Absorber or H2 target
S0 S1 S2 S3
Gas Cerenkov Counter
M2
M3
8"-bore doublet quadrupole
4" by 12" by 60" bending magnet
8" by 18" by 36" bending magnet
Concrete and paraffin shielding
6" Be target
48"
SCALE

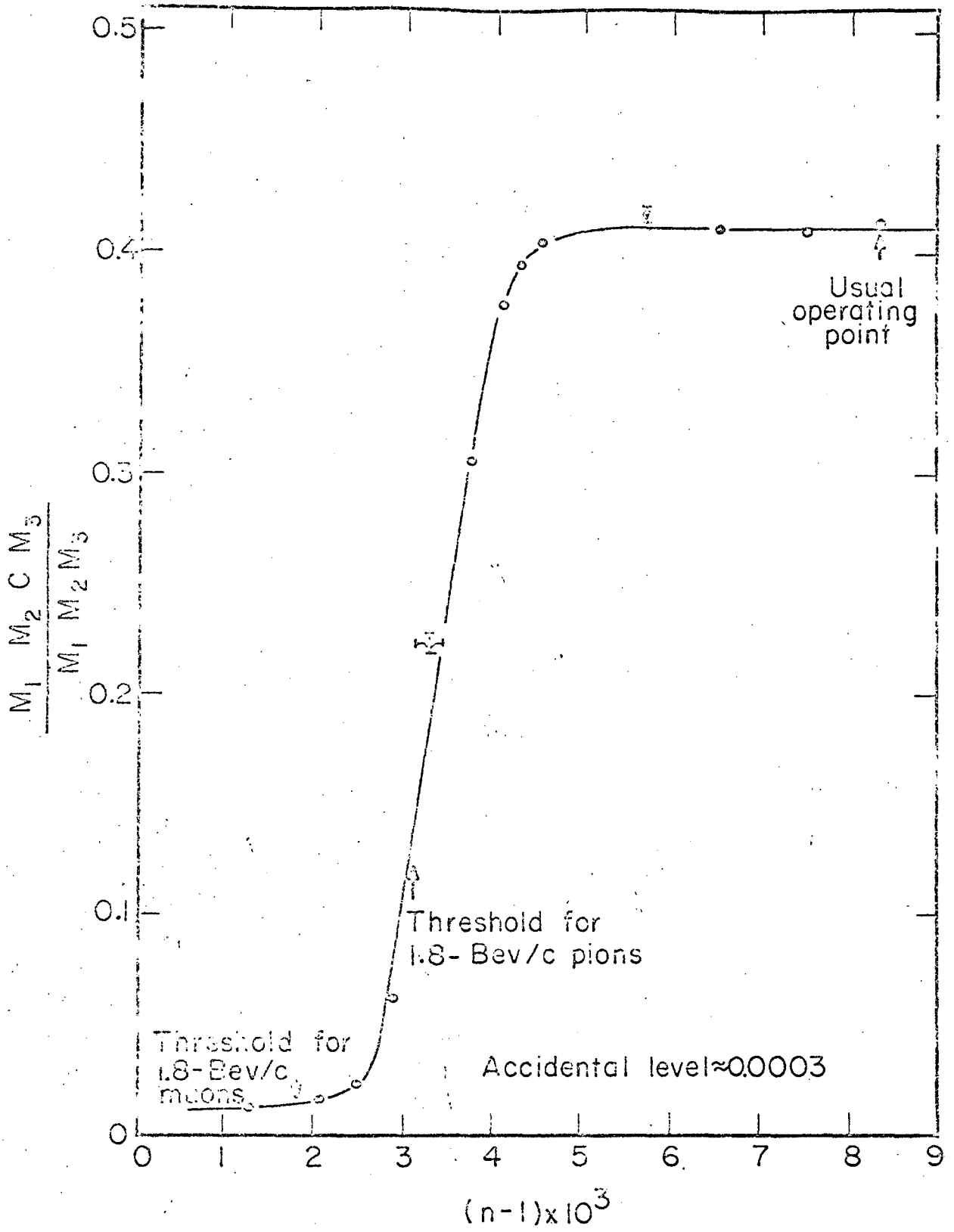
0.5
0.4
0.3
0.2
0.1
0
0 1 2 3 4 5 6 7 8 9
$\frac{M_1 M_2 C M_3}{M_1 M_2 M_3}$
(n-1)x10³
Usual operating point
Threshold for 1.8-Bev/c pions
Threshold for 1.8-Bev/c muons
Accidental level≈0.0003

Fig 3

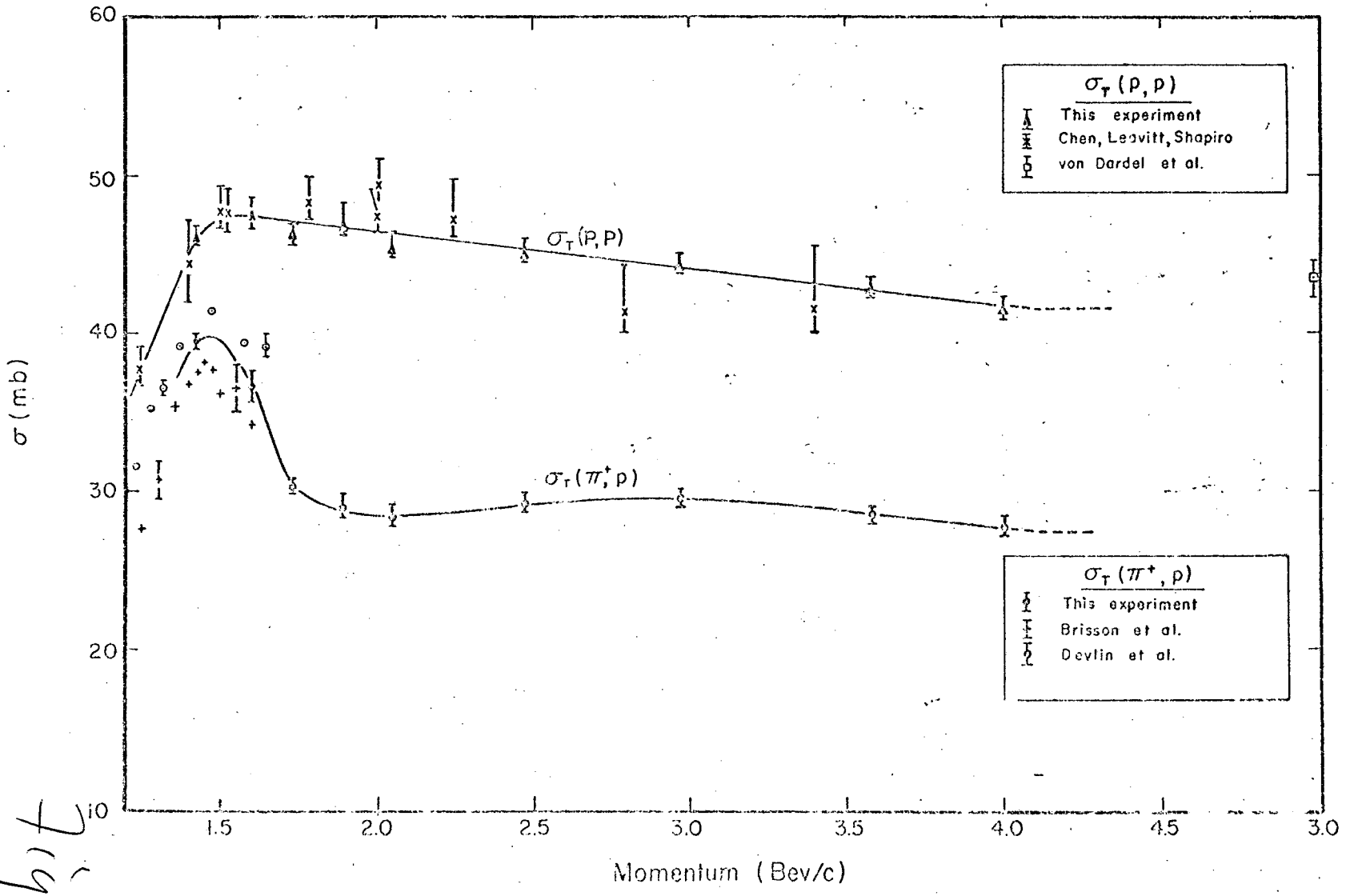
σ_T (p, p)
This experiment
Chen, Leavitt, Shapiro
von Dardel et al.
σ_T (P, P)
σ_T (π^+, p)
σ_T (π^+, p)
This experiment
Brisson et al.
Devlin et al.
σ (mb)
Momentum (Bev/c)
60
50
40
30
20
10
1.5
2.0
2.5
3.0
3.5
4.0
4.5
3.0

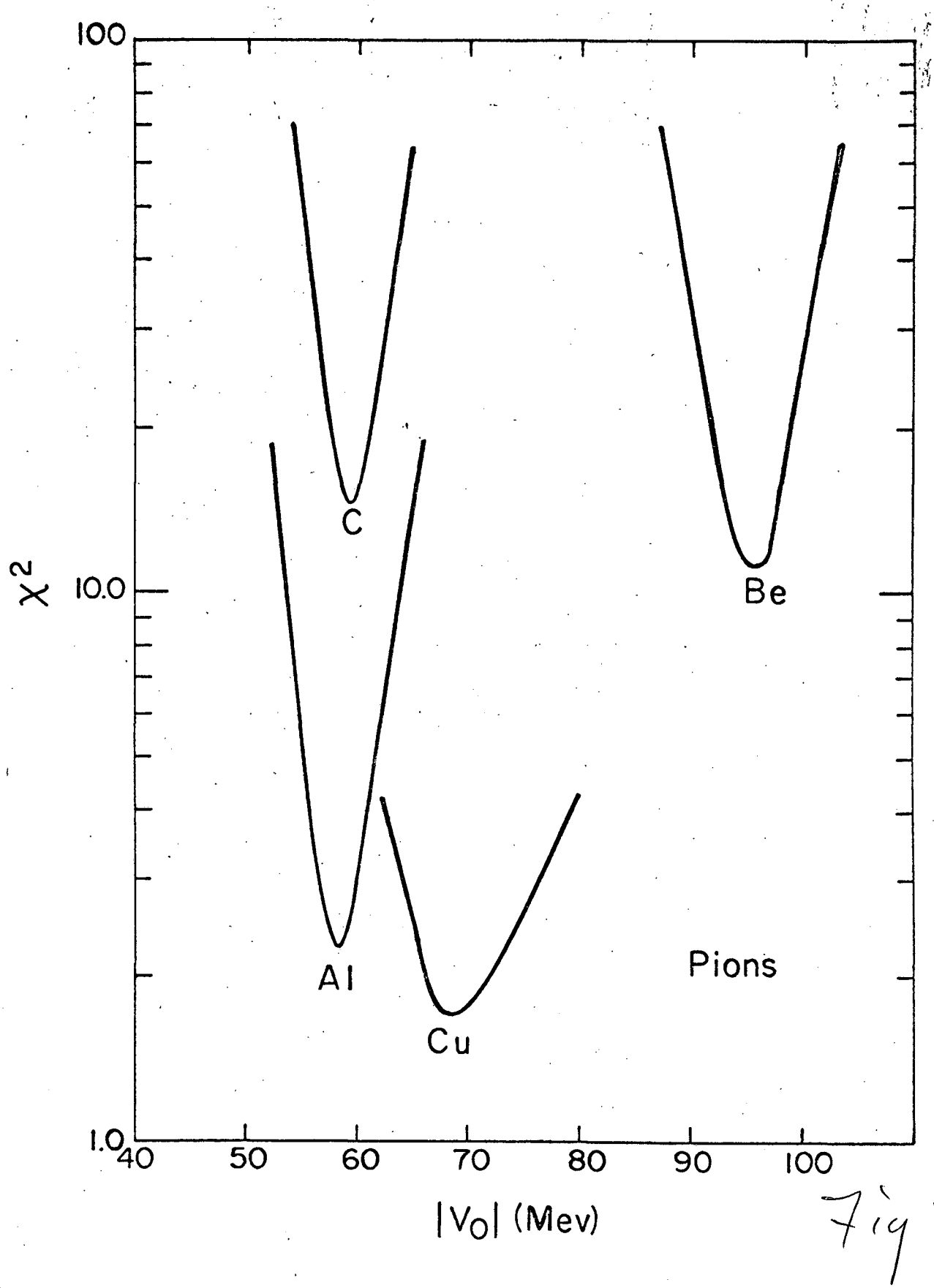

Fig 6

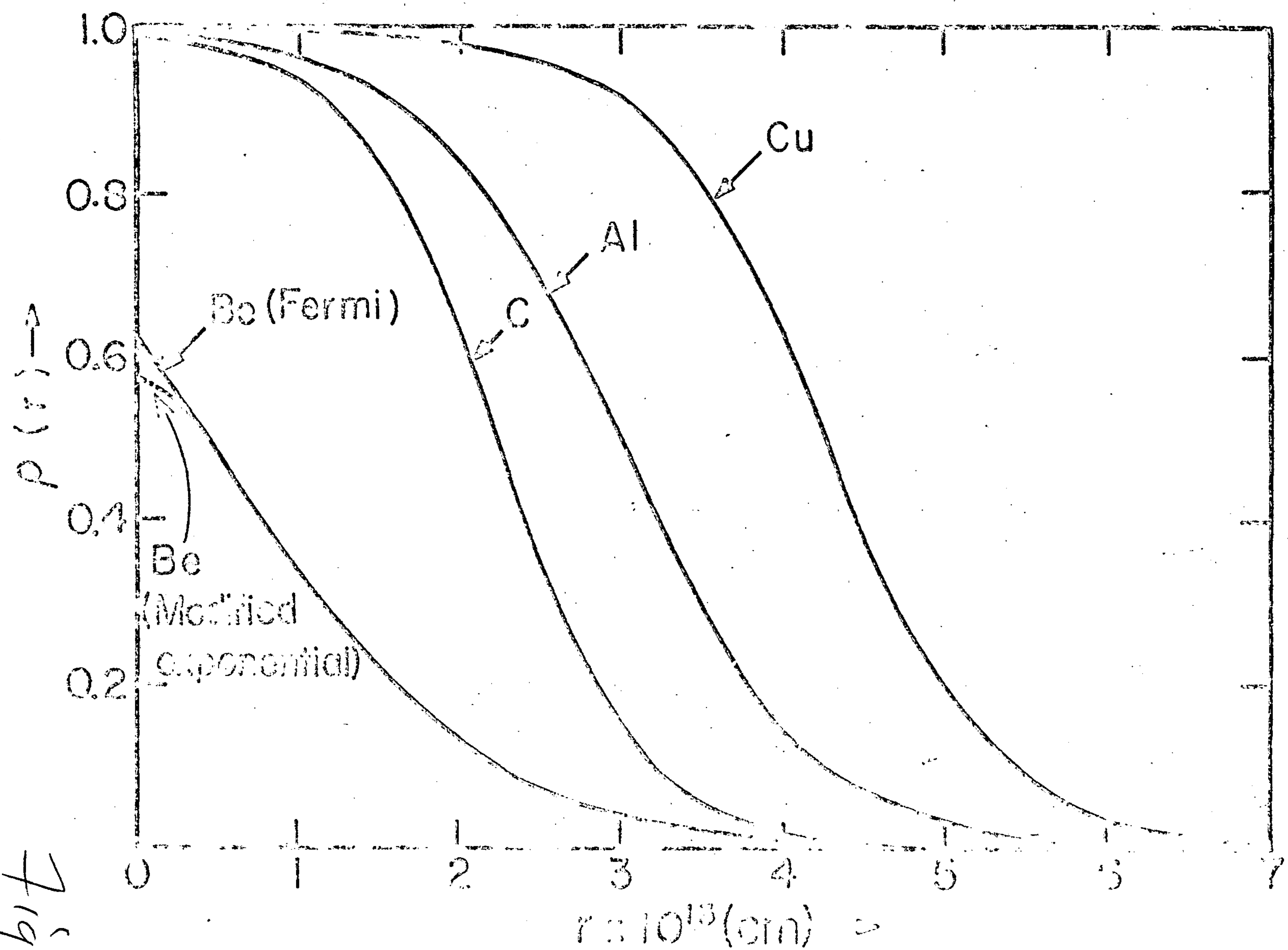
1.0
0.8
0.6
0.4
0.2
ρ (r) →
0
1
2
3
4
5
6
7
r x 10^13 (cm) →
Cu
Al
C
Be (Fermi)
Be
(Modified
exponential)

Fig 5

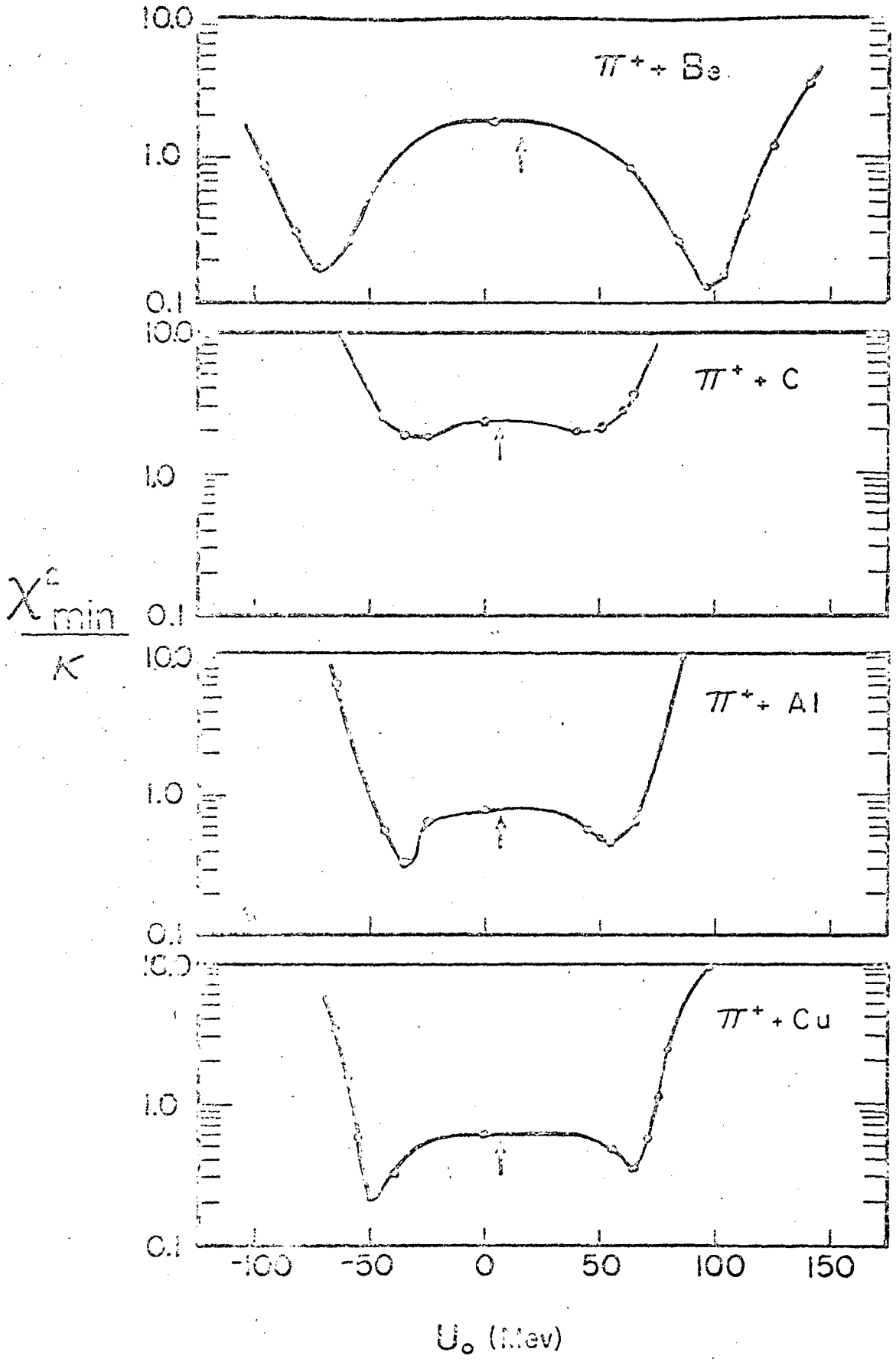
10.0
1.0
0.1
$\pi^+ + Be$
$\pi^+ + C$
$\pi^+ + Al$
$\pi^+ + Cu$
$\frac{\chi^2_{min}}{K}$
-100
-50
0
50
100
150
U_o (Mev)

Fig 8

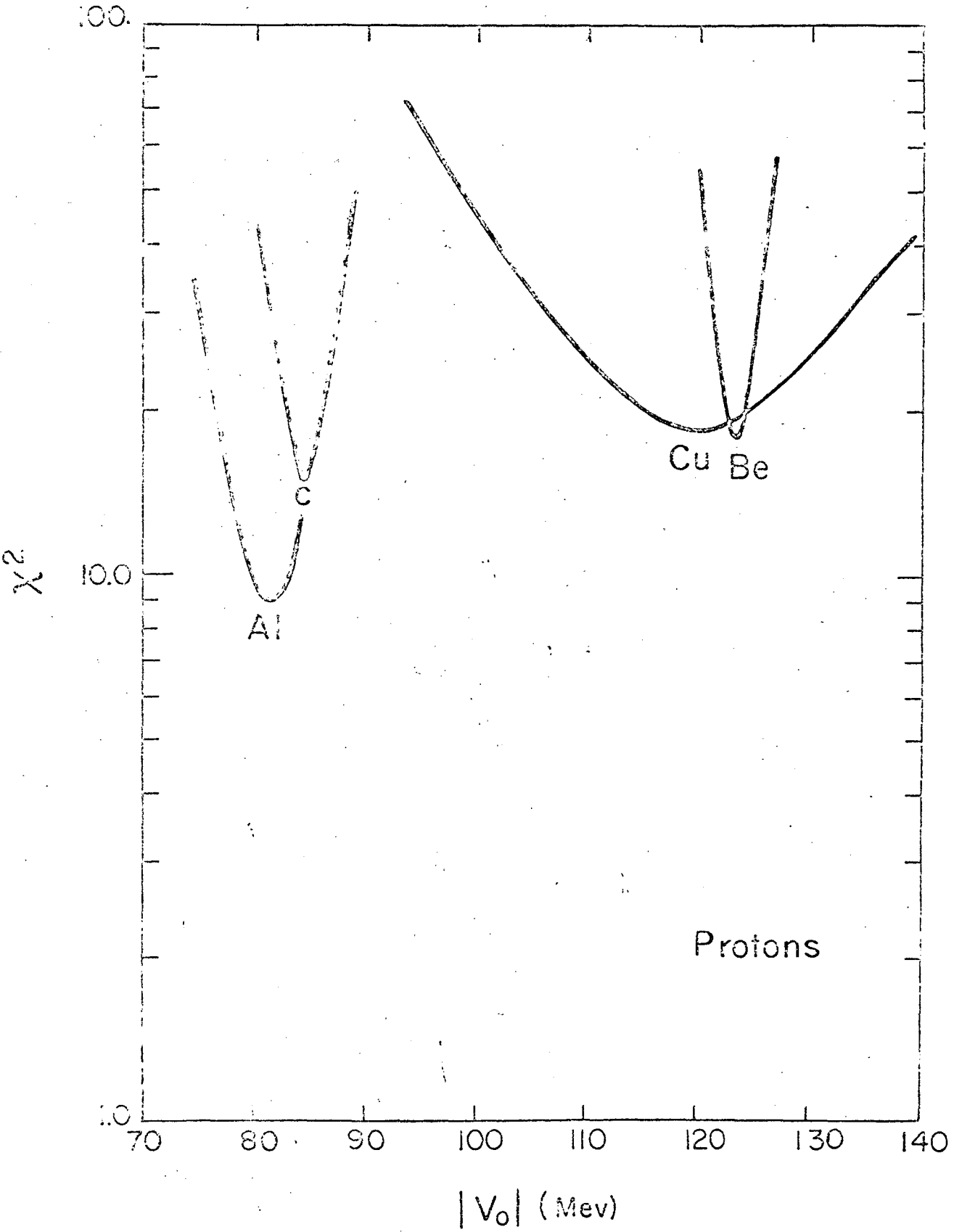
100.
10.0
1.0
χ^2
Al
C
Cu
Be
Protons
70
80
90
100
110
120
130
140
$|V_0|$ (Mev)

Fig 7

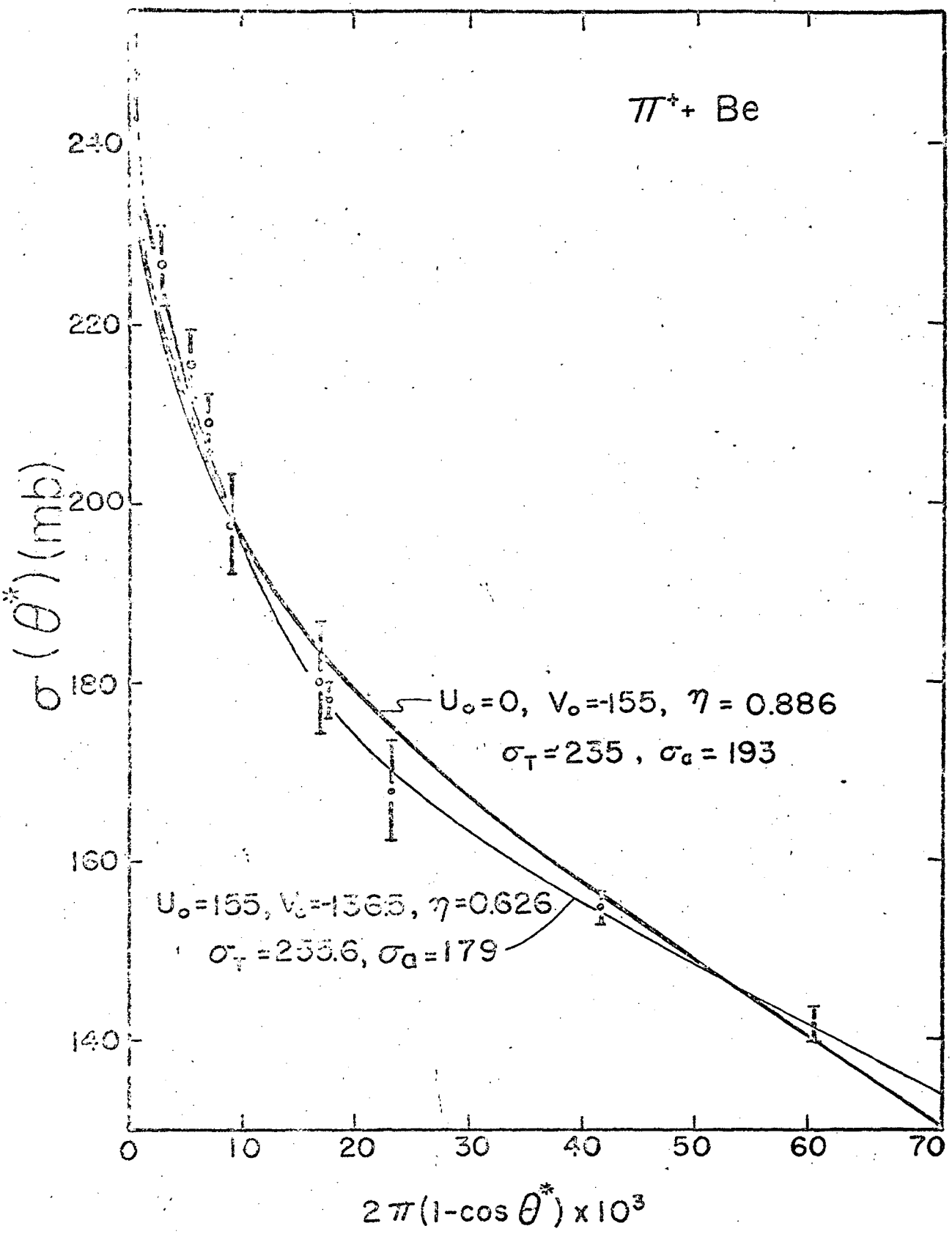
π^+ + Be
240
220
200
180
160
140
$\sigma(\theta^*)$ (mb)
$U_o = 0,\ V_o = -155,\ \eta = 0.886$
$\sigma_T = 235,\ \sigma_a = 193$
$U_o = 155,\ V_o = -136.5,\ \eta = 0.626$
$\sigma_T = 233.6,\ \sigma_a = 179$
0
10
20
30
40
50
60
70
$2\pi(1-\cos\theta^*) \times 10^3$

Fig 9